A New Model for Nuclear Envelope Breakdown ⱽ

Mark Terasaki,*† Paul Campagnola,* Melissa M. Rolls,‡ Pascal A. Stein,‡ Jan Ellenberg,§ Beth Hinkle,* and Boris Slepchenko*

*Department of Physiology, University of Connecticut Health Center, Farmington, Connecticut 06032; ‡Howard Hughes Medical Institute and Department of Cell Biology, Harvard Medical School, Boston, Massachusetts 02115; and §European Molecular Biology Laboratory, D-69117 Heidelberg, Germany

Nuclear envelope breakdown was investigated during meiotic maturation of starfish oocytes. Fluorescent 70-kDa dextran entry, as monitored by confocal microscopy, consists of two phases, a slow uniform increase and then a massive wave. From quantitative analysis of the first phase of dextran entry, and from imaging of green fluorescent protein chimeras, we conclude that nuclear pore disassembly begins several minutes before nuclear envelope breakdown. The best fit for the second phase of entry is with a spreading disruption of the membrane permeability barrier determined by three-dimensional computer simulations of diffusion. We propose a new model for the mechanism of nuclear envelope breakdown in which disassembly of the nuclear pores leads to a fenestration of the nuclear envelope double membrane.

INTRODUCTION

The nuclear envelope is a double-membrane barrier that is continuous with the endoplasmic reticulum (ER). Entry into and exit from the nucleus is through the nuclear pores. Molecules smaller than ~40,000 Da are able to diffuse freely through pores (Peters, 1983, 1984), but larger molecules must be specifically transported through the pores. The nuclear lamina, which is composed primarily of isoforms of the intermediate filament protein lamin, underlies the nuclear envelope.

The nuclear envelope is disassembled during mitosis in higher eukaryotic cells. By transmitted light microscopy, the smooth distinct outline suddenly becomes crumpled and indistinct. The time at which this occurs is called nuclear envelope breakdown and is defined as the end of prophase and beginning of prometaphase. After nuclear disassembly has occurred, the lamins and peripheral proteins of the nuclear envelope are soluble in the cytoplasm (Gerace and Blobel, 1980). It was originally thought that the nuclear envelope and ER become vesiculated during mitosis, but it now appears that the ER remains continuous in most cells (Ellenberg *et al.*, 1997; Zaal *et al.*, 1999; Terasaki, 2000) and that the integral membrane proteins of the nuclear envelope, such as lamin receptors and integral membrane nuclear pore proteins, are dispersed throughout the ER (Ellenberg *et al.*, 1997; Yang *et al.*, 1997).

The process of nuclear envelope breakdown is triggered by active maturation-promoting factor (MPF), which is thought to be a complex of cyclin B and cdc2/cdk1 kinase. MPF moves into the nucleus where it directly phosphorylates or causes the phosphorylation of several targets (Gallant and Nigg, 1992; Ookata *et al.*, 1992; Collas, 1999). The lamins are among the first and most clearly demonstrated target of MPF. Phosphorylation of polymerized lamins causes depolymerization in vitro (Peter *et al.*, 1990; Ward and Kirschner, 1990), and expression of mutant lamins lacking phosphorylation sites interferes with nuclear lamina disassembly in living cells (Heald and McKeon, 1990). These experiments showed that phosphorylation is required for lamina disassembly and that lamina disassembly is required for normal mitosis, but it has not been demonstrated that lamina disassembly is required for disruption of the nuclear envelope membrane permeability barrier (see DISCUSSION). Likewise, a mechanism by which lamina disassembly could cause the disruption of the membrane barrier has not been established.

Starfish oocytes offer several experimental advantages for investigating nuclear envelope breakdown. The oocytes are optically clear and have a large nucleus, termed the germinal vesicle (GV). The GV breaks down 20–30 min after application of the maturation hormone 1-methyladenine (1-MA). It is also feasible to express exogenous proteins by mRNA injection. Results from this system lead us to propose a new model for the mechanism of nuclear envelope breakdown in which nuclear pore disassembly has a central role.

MATERIALS AND METHODS

Starfish (*Asterina miniata*) were obtained from Bodega Bay, CA. Oocytes were injected quantitatively using mercury pipets

* Corresponding author. E-mail address: terasaki@neuron.uchc.edu.

(Hiramoto, 1962; Terasaki and Jaffe, 1993; for more details on microinjection, see http://egg.uchc.edu/injection). To induce maturation, oocytes were exposed to 1 μM 1-MA (Sigma, St. Louis, MO).

For the experiment shown in Figure 2, the oocytes were imaged with a two-photon microscope. A Mira 900-F titanium-sapphire laser pumped by an Ar ion laser at 8 W all lines visible (Coherent Laser Group, Santa Clara, CA) was mode locked at 76 MHz and coupled with an MRC 600 scan head (Bio-Rad, Cambridge, MA) in which three dielectric mirrors had been replaced with aluminum mirrors. To image the rhodamine dextran-labeled oocytes, the laser was tuned to 830 nm with 20 mW of average power. A 20× N.A. 0.75 Plan-Neofluar (Zeiss, Thornwood, NY) objective lens was used. The scan parameters were zoom 2 and half-size box. For all other experiments, imaging was done with an MRC 600 confocal microscope coupled with an upright microscope (Axioskop, Zeiss), using a krypton argon laser. A Zeiss 40× N.A. 1.3 Plan-Neofluar objective lens was used for imaging.

Fluorescent dextrans were obtained from Molecular Probes (Eugene, OR) and were kept as stock concentrations of 5–10 mg/ml in injection buffer (100 mM potassium glutamate, 10 mM HEPES, pH 7). Methods for expressing XXXX (GFP) chimeras by mRNA injection were similar to that described previously (Terasaki *et al.*, 1996). RanGAP-GFP mRNA was transcribed in vitro using an mMessage mMachine kit (Ambion, Austin, TX). After injection of ~10 μg/ml (final concentration) mRNA, oocytes were incubated overnight at 18–20°C for expression.

For double-labeling experiments (Figure 4), 70-kDa tetramethyl rhodamine dextran was injected into RanGAP-GFP–expressing oocytes at a final concentration of 25 μg/ml. The oocytes were imaged using the K1 K2 filter set. The confocal microscope was set to collect images every 7 s. The excitation filter wheel was switched manually between the 488- and 568-nm band pass filters so that the GFP and rhodamine images were collected separately at 14-s intervals. The single excitation resulted in a brighter image of GFP than is obtained with the filters for dual excitation. The oocytes were imaged with a 40× N.A. 1.3 Plan-Neofluar objective lens. The image data was analyzed by the public domain National Institutes of Health Image program (available at http://rsb.info.nih.gov/nih-image/) and Kaleidagraph software (Synergy Software, Reading, PA).

For determining the permeability coefficient for 70-kDa entry during the first phase, data on the 70-kDa fluorescence in the GV were normalized so that the initial value was 0 and the final value was 1. For converting the exponential recovery constant k to permeability coefficient, the equation $k = 3P/R$ was used (Peters, 1984), where P is the permeability coefficient and R is the radius of the starfish nucleus (35 μm). For calculating the permeability coefficient for the 70-kDa dextran entry data, we used the equation: rate of change of concentration = $3Pg/R$, where g = concentration gradient. The flux was determined by measuring the slope of dextran entry at each time point.

Computer simulations of 70-kDa dextran diffusion were done using the "Virtual Cell" modeling environment (http://nrcam.uchc.edu). The expanding hole was modeled with the formula $S = 2\pi R^2(1 - \cos \theta)$, where S is the area of a permeable portion of the surface, $\theta = \pi t/T$, t is the current time, and T is the time at which the entire surface becomes permeable (in these simulations we used $T = 35$ s). This results in a steadily opening hole. Some trials with a nonlinear opening gave results that were less consistent with the data. The Virtual Cell model descriptions used for the GVBD simulations are available at http://room2.mbl.edu/gvbd/. We used a diffusion coefficient for 70-kDa dextran in cytosol of 20 μm^2 s^{-1}; this was obtained by extrapolating from the known values for small sugars (Weast, 1972) based on the relationship that diffusion coefficient is inversely proportional to the cube root of the molecular weight and then reducing this value fourfold, which is the ratio of the viscosity of cytosol to that of water (Luby-Phelps *et al.*, 1986).

RESULTS

Organization in the Immature Oocyte

Fully grown starfish oocytes are arrested in prophase of meiosis I. They have a diameter of 170–180 μm and a large nucleus, 50–70 μm in diameter, which is called the GV. Meiotic maturation is induced by the hormone 1-MA (Kanatani *et al.*, 1969). By transmitted light microscopy, the GV outline suddenly becomes less distinct ~20–30 min after application of 1-MA. The term "GV breakdown" (GVBD) refers to the time when the outline suddenly changes.

Compared with the oocytes of many other species, starfish oocyte maturation is rapid. This is reflected in the precocious positioning of the GV and centrosomes in the immature starfish oocyte. The GV is already located within 5 μm of the surface at the "animal pole" (Figure 1). The animal pole is the location on the egg surface where the polar bodies (the products of the meiotic divisions) are extruded; the "vegetal pole" is at the exact opposite location. The centrosomes are also already at the animal pole in the small region between the oocyte surface and GV (Otto and Schroeder, 1984). The GV envelope, which appears smooth elsewhere, is thrown into folds near the centrosomes. When loaded in an injection/observation chamber, the oocytes are found with animal-vegetal axis oriented in all directions. For most experiments, we used oocytes with their animal-vegetal axis oriented parallel to the coverslip; in this orientation, the animal and vegetal poles are in the same plane of focus, and the GV is seen from the side as in Figure 1.
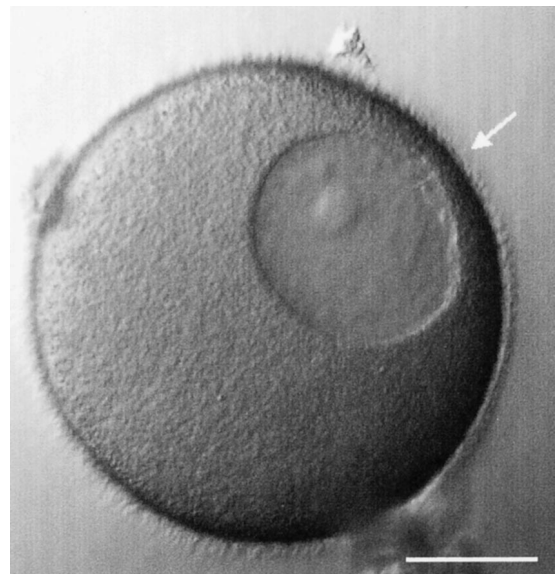

Figure 1. Organization of the immature starfish oocyte. The large GV (nucleus) is positioned near the oocyte surface at the animal pole (arrow). The centrosomes are located in the small region between the GV and the animal pole. The GV has a circular cross section when viewed along the animal-vegetal axis but is often slightly flattened when viewed perpendicularly to that axis. Approximately one-half of the cytoplasmic space is occupied by the yolk platelets, which are oval-shaped organelles with dimensions of 1–2 μm. The GV breaks down during meiotic maturation: see movie "gvbdt.mov" at the Molecular Biology of the Cell web site. Bar, 50 μm.
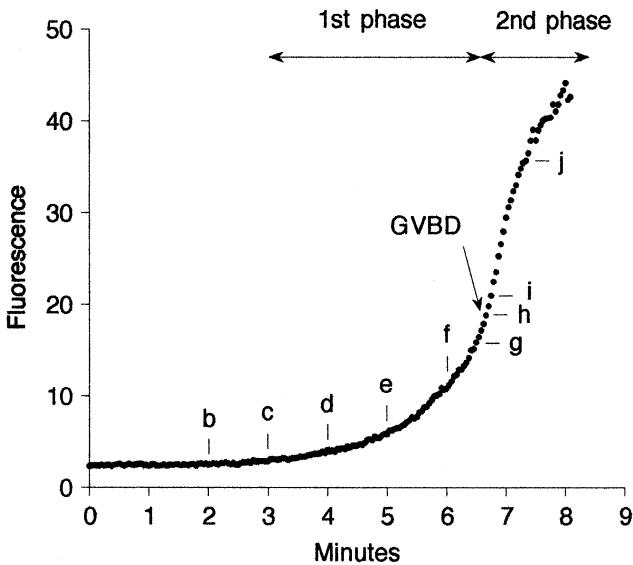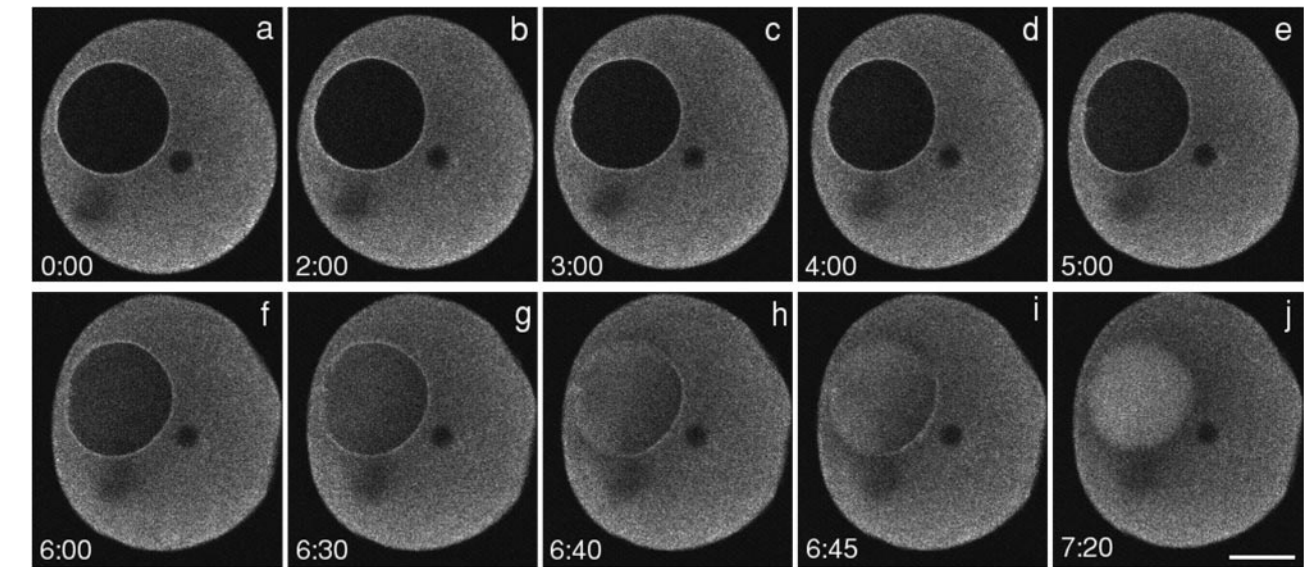
Figure 2. Dextran (70 kDa) entry during GVBD. Rhodamine dextran (70 kDa) was injected into the cytosol and imaged by a two-photon microscope at 2.5-s intervals. This image sequence was begun 10–15 min after addition of the maturation hormone 1-MA. Timing relative to the first image is shown on each image (minutes: seconds). There is an initial phase of slow entry followed by a massive entry from one region of the nuclear envelope at the time of GVBD (between g and h). The wave front develops a concave shape. See movie "2pgvbd.mov" at the Molecular Biology of the Cell web site. The small dark circle to the right of the GV is an oil drop introduced by microinjection; another oil drop out of the plane of focus accounts for the dark region beneath the GV. Bar, 50 μm. Graph, from this image sequence, the average fluorescence intensity of a 30- $\times$ 30-μm region at the center of the GV was determined. The time points corresponding to those shown in the image sequence are indicated by the lower case letters.

Starfish GVBD: Two Phases of 70-kDa Dextran Entry

Fluorescent 10-kDa dextran injected into the cytoplasm crosses the intact GV envelope, whereas 70-kDa dextran does not. This is consistent with a size cutoff of ~40 kDa for passive diffusion through nuclear pores, as seen in many other cells. We previously documented fluorescent 70-kDa dextran entry during maturation and found two phases of entry (Terasaki, 1994). The first phase is a slow increase throughout the GV, lasting 3–5 min. The second phase is a massive wave at the time of GVBD. Usually this originated from the animal side of the GV, although sometimes the 70-kDa dextran entered from the sides, perpendicular to the animal-vegetal axis (see Figure 4); oocytes from a given animal tended to have the same entry pattern.

Using a two-photon microscope, we were able to improve the time resolution of the image sequences to 2.5-s intervals (Figure 2; see accompanying movie). The 70-kDa dextran enters as a massive wave, taking ~45 s to fill the nuclear space. In the later stages of the entry, the wave clearly has a concave wave front. The fluorescence eventually becomes brighter in the interior of the GV than in the cytoplasm. This is due to the absence of organelles in the nucleus, whereas the cytoplasm has many yolk platelets ~1–2 μm in diameter that occupy a large fraction of the cytosolic space. The average cytoplasmic fluorescence is ~0.5 times the brightness of the nucleoplasmic fluorescence even though the cytosolic and nucleoplasmic dextran concentrations are the same (Terasaki, 1994). Another feature of the experimental data is
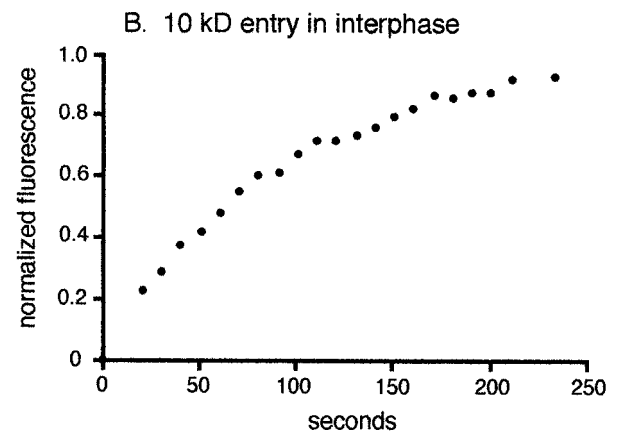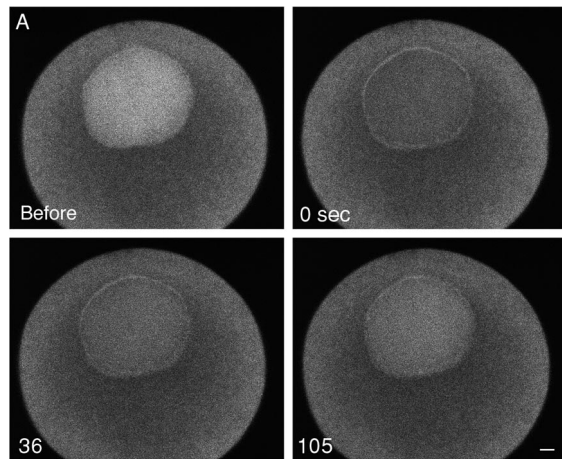
Figure 3. Permeability of the GV envelope in interphase and in the period before GVBD. (A) Fluorescein dextran (10 kDa) was injected into the cytoplasm of an immature oocyte and was allowed to equilibrate across the GV envelope. Fluorescence in the GV interior was partially photobleached, and the recovery of fluorescence due to diffusion through nuclear pores was imaged. Bar, 50 μm. (B) The average fluorescence intensity in a small region in the GV was determined. The data were fit well by an exponential recovery, corresponding to a permeability coefficient of ~0.15 μm/s. (C) Permeability of the GV envelope for 70-kDa dextran in the period before GVBD. The permeability coefficient is not constant and was determined for each time point by measuring the slope of the line from a graph like that in Figure 2 and then dividing by the gradient of 70-kDa dextran across the GV envelope. The average value for the permeability coefficient just before GVBD was 0.04 μm/s. The similarity of this value to the permeability of 10-kDa dextran through nuclear pores in the immature oocyte is consistent with entry of 70-kDa through altered nuclear pores with an increased pore size cutoff.
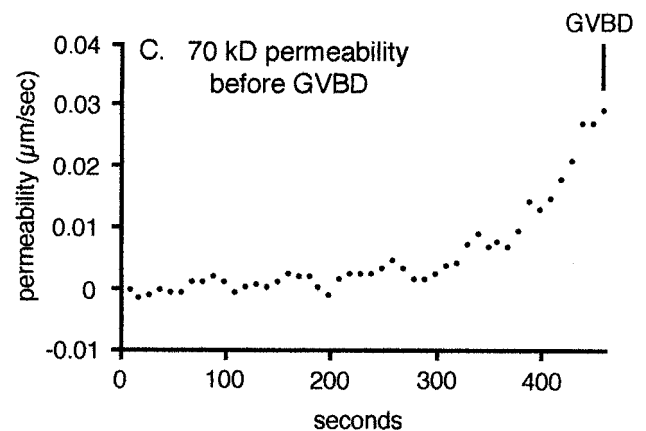
a temporary darkened zone in the cytoplasm bordering theGV, which is apparently due to local depletion of dextran that has entered the nuclear region (see Figure 2j).

Evidence That the First Phase Is Due to Disassembly of Nuclear Pores

To test whether the first phase of 70-kDa dextran entry is due to changes in nuclear pore permeability, we quantitated nuclear envelope permeability during this period and also imaged a GFP chimera of a nuclear pore protein.

Methods for quantitating diffusion through nuclear pores have been established by Peters (1984). Small fluorescent dextrans injected into the cytosol cross the nuclear envelope and come to equilibrium. The fluorescence within the nucleus is photobleached, and the recovery of fluorescence in the nucleus is monitored. The recovery is exponential, because the entry is driven by the concentration gradient of unbleached fluorescent dextran between cytoplasm and nucleus, which gradually becomes reduced as more dextran enters the nucleus. The permeability coefficient, which is the ratio of movement across the barrier to the concentration gradient, can be calculated from the recovery data (Peters, 1984).

The permeability coefficient for the movement of 10-kDa dextran through the nuclear pores of the GV envelope of immature oocytes was determined, and this permeability was then compared with the entry of 70-kDa dextran during the first phase. If the permeabilities for these two processes differed widely, it would provide evidence against diffusion of 70-kDa dextran through nuclear pores. Fluorescent 10-kDa dextran was allowed to come to equilibrium between the cytosol and GV. The fluorescence within the GV was photobleached, and the recovery of GV fluorescence was monitored (Figure 3A). The recovery curve, which "opens downward" (Figure 3B), was fit well by an exponential recovery. The permeability coefficient of the immature oocyte nuclear envelope to 10-kDa dextran was 0.15 ± 0.02 μm/s (SD, $n = 5$).

The 70-kDa dextran entry during the first phase does not follow an exponential recovery (Figure 2, graph). The curve "opens upward," which indicates that the permeability coefficient is not constant but instead is increasing with time. To obtain quantitative values for the changing permeability, the slope of the curve at each time point (of a graph similar to that shown in Figure 2) was divided by the difference in concentration between cytoplasm and GV at that time point. The data show a steadily increasing permeability, which reached a value of 0.040 ± 0.009 μm/s ($n = 3$) just before GVBD (Figure 3C).

The permeability coefficient of 70-kDa dextran just before GVBD is of similar magnitude as the permeability of 10-kDa
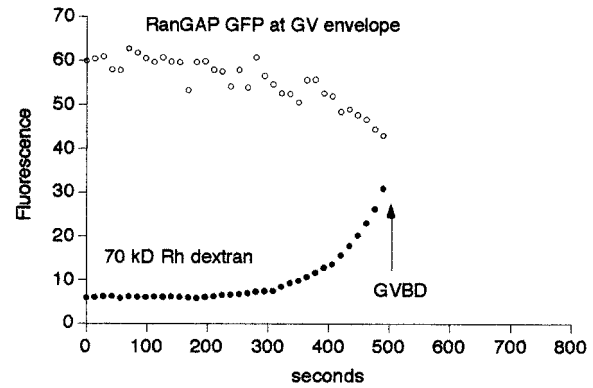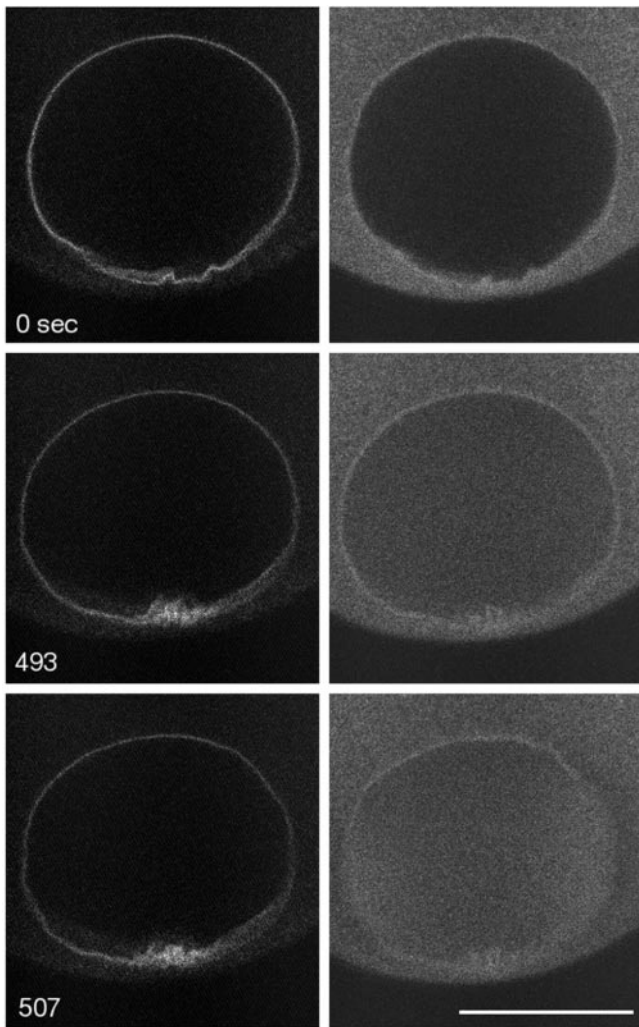
Figure 4. Kinetics of a nuclear pore GFP chimera during GVBD. RanGAP is a peripheral protein of the nuclear pore. RanGAP-GFP was expressed by mRNA injection, and the following day, 70-kDa rhodamine dextran was injected into the oocytes. RanGAP-GFP (left) was imaged alternately with 70-kDa rhodamine dextran (right) during maturation at 7-s intervals so that each fluorescent marker was imaged at 14-s intervals (see MATERIALS AND METHODS for more details). As shown by 70-kDa dextran entry, GVBD occurred at ~507 s. RanGAP-GFP fluorescence at the nuclear rim just before GVBD at 493 s has decreased noticeably from the 0-s time point. In this oocyte, the 70-kDa dextran begins to enter at the sides of the GV rather than in the animal pole region. See movie "rangap.mov" at the Molecular Biology of the Cell web site. Bar, 50 μm. The graph shows fluorescence of RanGAP-GFP in the nuclear rim and of 70-kDa dextran in the GV interior. RanGAP-GFP fluorescence decreases significantly before GVBD and seems to decrease with approximately the same time course as the first phase of 70-kDa dextran entry. This is evidence that the nuclear pores are being disassembled before GVBD and that 70-kDa dextran enters through nuclear pores whose cutoff has been increased.

dextran across the intact GV envelope (0.04 vs. 0.15 μm/s). This means that the 70-kDa dextran is moving across the GV envelope with approximately the same ease as 10-kDa dextran diffuses through nuclear pores in interphase. This supports the idea that the first phase of entry of 70-kDa dextran is through nuclear pores whose size cutoff has increased.

To attempt to obtain more direct evidence of the status of nuclear pores just before GVBD, we imaged a GFP chimera expected to localize to the nuclear pore. RanGAP1 is found on the cytosolic side of nuclear pores and is responsible for GTPase activation of Ran involved in nuclear import and export. "RanGAP-GFP" (VLP 35; Rolls *et al.*, 1999) consists of an N-terminal GFP followed by the C-terminal 190 amino acids of human RanGAP1; it is thus missing the N-terminal 397 amino acids. RanGAP-GFP localizes to the nuclear envelope of human cultured cell lines (Rolls *et al.*, 1999). RanGAP-GFP was expressed in starfish oocytes by injection of mRNA. After the sample was incubated overnight, fluorescence was seen at the GV envelope. Individual pores could not be resolved, which is expected because electron micrographs show a high density of 50 nuclear pores/μm² in the starfish GV (Art Hand, unpub-

lished observations). Expression of RanGAP-GFP in starfish oocytes had no noticeable effect on the timing or normally occurring events of meiotic maturation.

Immature oocytes expressing RanGAP-GFP were injected with 70-kDa rhodamine dextran and were then exposed to maturation hormone and imaged by double-labeling techniques. The onset of the second phase of 70-kDa dextran entry allowed us to determine the time of GVBD (Figure 4; see accompanying movie). In the parallel images, the RanGAP fluorescence was stable and then began to decrease a few minutes before GVBD (3/3 oocytes). This provides evidence that nuclear pores start to become disassembled before GVBD.

The Second Phase Is Due to Disruption of the Membrane Barrier

Because the second phase was a massive wave, we thought that this should correspond to the complete disruption of part of the double-membrane barrier. To test this, we made three-dimensional simulations of 70-kDa dextran entry using the "Virtual Cell" modeling environment (Schaff *et*

al.,1997). Space was divided up into small cubes, which were assigned initial concentration values (finite volume discretization). The passage of material between neighboring cubes was calculated in small time increments according to the diffusion equation (i.e., flux is linearly proportional to the concentration difference). For these simulations, we used cubes with 2-μm sides and a time step of 20 ms. We also used a diffusion coefficient of 20 μm^2/s for the 70-kDa dextran (see MATERIALS AND METHODS).

We started by simulating dextran entry through a large fixed diameter hole in the GV envelope. All simulations with a fixed sized hole were unable to reproduce the observed entry pattern. Even if the dextran entered through a hole with a radius of 22 μm (63% of the GV radius), it did not fill the GV at 4 min, and the wave front shape began and remained convex (Figure 5; see accompanying movie). This prompted us to suppose that the dextran was entering through an expanding hole rather than a hole of fixed size. We tested a model in which a hole expands at a steady rate (see MATERIALS AND METHODS). These simulations yielded a better fit to the data (Figure 5).

To account for the reduced cytosolic space compared with the nucleoplasmic space, we introduced a correction factor in which fluorescence was twice as bright for the same concentration in the nucleus. We were also interested to reproduce the depletion zone outside the GV. The depletion was negligible when we used a diffusion coefficient of 20 μm^2/s for both cytoplasm and nucleus. A better fit was obtained when the diffusion coefficient in the cytoplasm was reduced to 3 μm^2/s; a lower cytoplasmic coefficient is reasonable given the abundant large yolk platelets in the cytoplasm that hinder the free diffusion paths. An expanding hole that spreads over the GV envelope in 35 s generated a concave wave that fills the GV in approximately the same time as observed experimentally, and a reduced cytoplasmic diffusion coefficient of 3 μm^2/s results in a good fit for the depletion zone around the GV (Figure 5). In this simulation, the disruption spreads at a rate of ~3 μm/s.

On the basis of these simulations, we looked at transmitted light microscopic sequences of GVBD for a spreading change in the outline of the GV. There is a change that can be seen in movie sequences played forward and backward repeatedly, but this change is difficult to document in still images (see movie that accompanies Figure 1). We conclude that the GV membrane bilayer barrier is disrupted in a progressive manner.

DISCUSSION

Fluorescent 70-kDa dextran, which does not diffuse passively through nuclear pores, was previously used to characterize nuclear envelope breakdown in living cells (Terasaki, 1994). There were two phases of entry, a slow increase and an abrupt wave. It was suggested that the second phase corresponded to disruption of the membrane permeability barrier and that the first was due to increased nuclear pore permeability.

We examined the first phase of 70-kDa entry quantitatively. The permeability increased with time and reached a value of 0.04 μm/s just before GVBD. This value is of the same order of magnitude as the permeability of 0.15 μm/s for the entry of 10-kDa dextran for the intact GV envelope and provides support for the idea that the 70-kDa molecules are entering through nuclear pores with an increased size cutoff. We also imaged a GFP chimera of RanGAP, which is expected to localize to the nuclear pores. RanGAP-GFP fluorescence at the GV
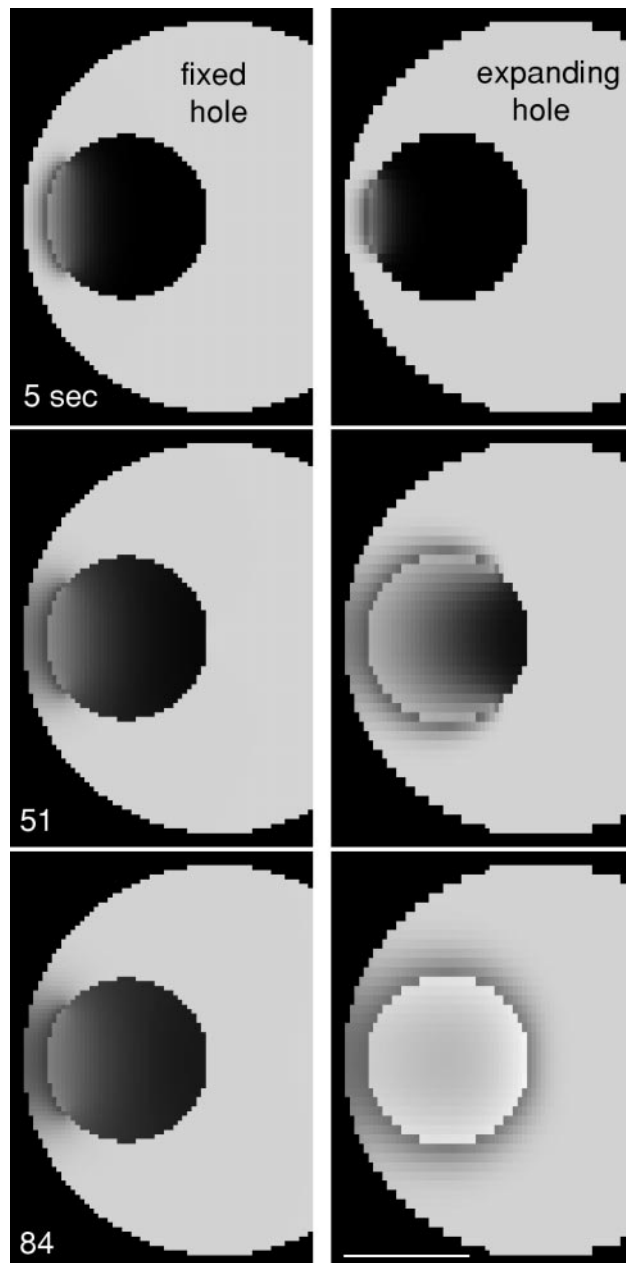

Figure 5. Simulation of 70-kDa entry at the time of GVBD. Left, simulation of entry through a hole with a fixed diameter of 45 μm. Right, simulation of entry through a hole that opens at a constant rate and is complete at 35 s. Timing of the images relative to the beginning of the opening in the simulation are shown. The simulations were done in three dimensions, and the equatorial plane is shown. The simulation with the expanding hole fits the experimental data (Figure 2) much better than the simulation with the fixed hole. See movies "fixed.mov" and "spreading.mov" at the Molecular Biology of the Cell web site. Bar, 50 μm.

envelope decreased before GVBD in parallel with the first phase of 70-kDa dextran entry. Our results support the idea that nuclear pore disassembly begins significantly before the time of nuclear envelope breakdown.

A recent study by Lee *et al.* (2000) localized nuclear envelope proteins by immunofluorescence in dividing cells of the Caenorhabditis *elegans* embryo. In these cells, which resemble embryonic cells of *Drosophila* (e.g., Stafstrom and Staehelin, 1984), the nuclear envelope breaks down in two stages, first near the mitotic poles, and then later, it is completely disassembled (in *C. elegans*, during anaphase). Lee *et al.* (2000) found that nucleoporins are released from the nuclear envelope significantly before the complete disassembly stage, although there were no data on pore disassembly before the first partial breakdown near the mitotic poles.

We used three-dimensional computer simulations to investigate the second phase of 70-kDa dextran entry in starfish oocytes. A good fit to the data was obtained with a spreading disruption of the membrane permeability barrier. The model was able to reasonably fit two other details, the depletion zone outside of the GV and the increased fluorescence in the GV due to the lack of yolk platelets. We conclude that the second phase is a spreading disruption of the membrane permeability barrier of the nuclear envelope.

Nuclear Pore Disassembly

The nuclear pore is a very complex structure; a recent study analyzed the structure in yeast in great detail (Rout *et al.*, 2000). The proteins are organized into different structural components of the pore: the spoke ring complex, the central pore complex responsible for transport, which fits inside the spoke ring complex, and peripheral structures to the pore, which are the basket on the nuclear side and the filaments on the cytoplasmic side.

Some studies have suggested that mitotic kinases control disassembly of the pores. Macaulay *et al.* (1995) found that two of the three major glycoprotein components of the pore (p200 and p97) are highly phosphorylated during mitosis in vitro and in vivo. Interestingly, these glycoproteins are part of higher molecular weight complexes that appear to remain together during mitosis and may represent modules for assembly and disassembly of pores. Favreau *et al.* (1996) found that the soluble Nup 153, 214, and 358 are phosphorylated in interphase and become hyperphosphorylated in mitosis.

A New Model

We propose a new model for the mechanism of nuclear envelope breakdown (Figure 6). Active MPF phosphorylates nuclear pore components, starting nuclear pore disassembly. At some point during the disassembly process, the ability of the nuclear pore to block diffusion of molecules >40 kDa is lost. However, the aqueous channel of the pore as well as the double membrane of the nuclear envelope remains intact, so that there is no bulk mixing of nucleoplasm and cytoplasm. This period corresponds to the first phase of 70-kDa dextran entry. When the membrane proteins making up the spoke ring complex have become loosened, the hole in which the complex sits becomes free to expand, resulting in large fenestrations in the GV envelope. This corresponds to the second phase of 70-kDa dextran entry. One advantage of this model is that it is consistent with the previous studies that nuclear envelope membrane proteins are within continuous membranes of the ER during mitosis rather than in vesicles (Ellenberg *et al.*, 1997; Yang *et al.*, 1997).

One uncertainty in our model is the propagation of the membrane disruption during the second phase of 70-kDa dextran
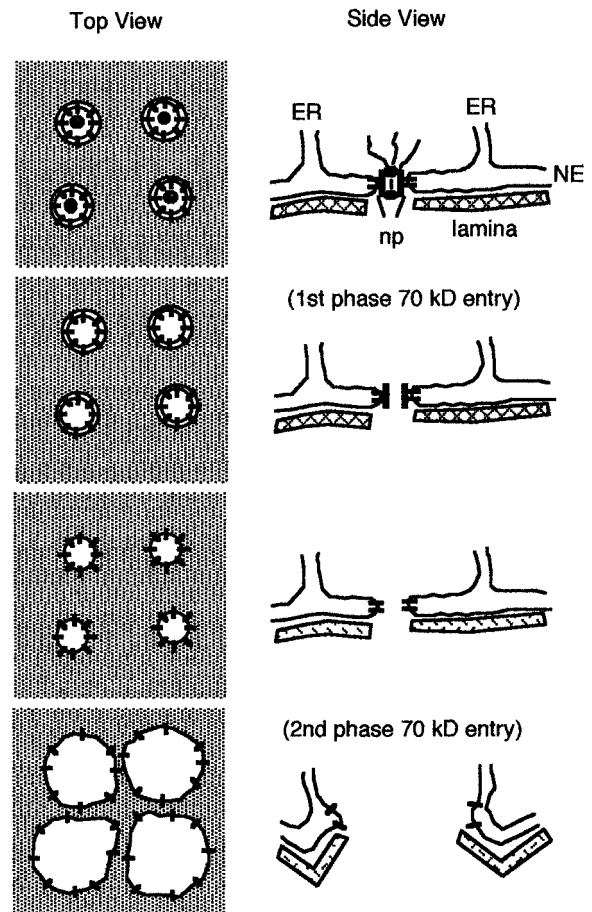

Figure 6. A new model for nuclear envelope (NE) breakdown. Active MPF enters the nucleus and begins a stepwise process of nuclear pore (np) disassembly. At some point, perhaps corresponding to loss of the central plug, larger molecules can diffuse through the pore; this is proposed to correspond to the first phase of 70-kDa dextran entry. The nuclear pores continue to be disassembled until the membrane hole in which they are located becomes destabilized, and the holes can begin to expand. In some unknown manner, the expansion of the holes is propagated throughout the nuclear envelope, resulting in a fenestrated membrane; this is proposed to correspond to the second phase of 70-kDa dextran entry. In this model, the nuclear envelope membranes remain continuous and are resorbed into the ER during mitosis. Nuclear lamina disassembly is required for normal mitosis and occurs at approximately the same time, but its role in the disruption of the nuclear envelope membrane barrier is uncertain.

entry. The time-lapse sequences and simulations suggest that the disruption of the nuclear envelope begins at one or two sites and proceeds at a relatively constant rate of a few micrometers per second. This could be due to a chemically propagated signal, such as an MPF activation wave (e.g., Perez-Mongiovi *et al.*, 1998), or to a physically propagated one; for instance, the nuclear envelope may be under tension and, once disrupted at a point, may undergo a process similar to popping a soap bubble.

Another uncertainty is how nuclear lamina disassembly is related to nuclear envelope breakdown. Experiments in cell-free extracts have suggested that lamin disassembly does not cause nuclear membrane disruption (Newport and Spann, 1987). Heald

and McKeon (1990) expressed lamins in which normal phosphorylation sites were mutated so that they were no longer able to be phosphorylated. In cells expressing single and double mutants, partial disassembly occurred, resulting in crumpled nuclear lamina. Abnormal spindles were still able to form so that the membrane permeability barrier must have been broken. Mitotic cells expressing a triple mutant had an intact lamina with no spindle. However, it is possible that the membrane barrier had been broken, and that the intact nuclear lamina prevented assembly of the spindle. Thus, nuclear lamina disassembly is required for normal mitosis, but disassembly has not yet been shown to be required for the disruption of the membrane permeability barrier. One possibility is that lamina disassembly is essentially independent of disruption of the membrane permeability barrier. Another possibility is that weakening of the lamina contributes to the propagation of the fenestrated membrane that we propose. These issues may be addressed by future studies with lamin mutants and GFP chimeras in starfish oocytes.

REFERENCES

Collas, P. (1999). Sequential PKC-, and Cdc2-mediated, phosphorylation events elicit zebrafish nuclear envelope disassembly. J. Cell Sci. *112*, 977–987.

Ellenberg, J., Siggia, E.D., Moreira, J.E., Smith, C.L., Presley, J.F., Worman, H.J., and Lippincott-Schwartz, J. (1997). Nuclear membrane dynamics and reassembly in living cells: targeting of an inner nuclear membrane protein in interphase and mitosis. J. Cell Biol. *138*, 1193–1206.

Favreau, C., Worman, H.J., Wozniak, R.W., Frappier, T., and Courvaline, J.-C. (1996). Cell cycle-dependent phosphorylation of nucleoporins and nuclear pore membrane protein gfp210. Biochemistry *35*, 8035–8044.

Gallant, P., and Nigg, E.A. (1992). Cyclin B2 undergoes cell cycle-dependent nuclear translocation and, when expressed as a non-destructible mutant, causes mitotic arrest in HeLa cells. J. Cell Biol. *117*, 213–224.

Gerace, L., and Blobel, G. (1980). The nuclear envelope lamina is reversibly depolymerized during mitosis. Cell *19*, 277–287.

Heald, R., and McKeon, F. (1990). Mutations of phosphorylation sites in lamin A that prevent nuclear lamina disassembly in mitosis. Cell *61*, 579–589.

Hiramoto, Y. (1962). Microinjection of live spermatozoa into sea urchin eggs. Exp. Cell Res. *27*, 416–426.

Kanatani, H., Shirai, H., Nakanishi, K., and Kurokawa, T. (1969). Isolation and identification of meiosis inducing substance in starfish *Asterias amurensis*. Nature *221*, 273–274.

Lee, K.K., Gruenbaum, Y., Spann, P., Liu, J., and Wilson, K.L. (2000). *C. elegans* nuclear envelope proteins emerin, MAN1, lamin, and nucleoporins reveal unique timing of nuclear envelope breakdown during mitosis. Mol. Biol. Cell *11*, 3089–3099.

Luby-Phelps, K., Taylor, D.L., and Lanni, F. (1986). Probing the structure of cytoplasm. J. Cell Biol., *102*, 2015–2022.

Macaulay, C., Meier, E., and Forbes, D.J. (1995). Differential mitotic phosphorylation of proteins of the nuclear pore complex. J. Biol. Chem. *207*, 254–262.

Newport, J., and Spann, T, 1987. Disassembly of the nucleus in mitotic extracts: membrane vesicularization, lamin disassembly, and chromosome condensation are independent processes. Cell *48*, 219–230.

Ookata, K., Hisanaga, S., Okano, T., Tachibana, K., and Kishimoto, T. (1992). Relocation and distinct subcellular localization of p34 cdc2-cyclin B complex at meiosis reinitiation in starfish oocytes. EMBO J. *11*, 1763–1772.

Otto, J.J., and Schroeder, T.E. (1984). Microtubule arrays in the cortex and near the germinal vesicle of immature starfish oocytes. Dev. Biol. *101*, 274–281.

Perez-Mongiovi, D., Chang, P., and Houliston, E. (1998). A propagated wave of MPF activation accompanies surface contraction waves at first mitosis in *Xenopus*. J. Cell Sci. *111*, 385–393.

Peter, M., Nakagawa, J., Doree, M., Labbe, J.C., and Nigg, E.A. (1990). In vitro disassembly of the nuclear lamina and M phase-specific phosphorylation of lamins by cdc2 kinase. Cell *61*, 591–602.

Peters, R. (1983). Nuclear envelope permeability measured by fluorescence microphotolysis of single liver cell nuclei. J. Biol. Chem. *258*, 11427–11429.

Peters, R. (1984). Nucleo-cytoplasmic flux and intracellular mobility in single hepatocytes measured by fluorescence microphotolysis. EMBO J. *3*, 1831–1836.

Rolls, M.M., Stein, P.A., Taylor, S.S., Ha, E., McKeon, F., and Rapoport, T.A. (1999). A visual screen of a GFP-fusion library identifies a new type of nuclear envelope membrane protein. J. Cell Biol. *146*, 29–44.

Rout, M.P., Aitchison, J.D., Suprapto, A., Hjertaas, K., Zhao, Y., and Chait, B.T. (2000). The yeast nuclear pore complex: composition, architecture, and transport mechanism. J. Cell Biol. *148*, 635–651.

Schaff, J., Fink, C.C., Slepchenko, B., Carson, J.H., and Loew, L.M. (1997). A general computational framework for modeling cellular structure and function. Biophys. J. *73*, 1135–1146.

Stafstrom, J.P., and Staehelin, L.A. (1984). Dynamics of the nuclear envelope and of nuclear pore complexes during mitosis in the *Drosophila* embryo. Eur. J. Cell Biol. *34*, 179–189.

Terasaki, M., and Jaffe, L.A. (1993) Imaging of the endoplasmic reticulum in living marine eggs. In: Methods in Cell Biology: Cell Biological Applications of Confocal Microscopy, vol. 38, ed. B. Matsumoto, Orlando, FL: Academic Press, 211-220.

Terasaki, M. (1994). Redistribution of cytoplasmic components during germinal vesicle breakdown in starfish oocytes. J. Cell Sci. *107*, 1797–1805.

Terasaki, M., Jaffe, L.A., Hunnicutt, G.R., and Hammer III, J.A. (1996). Structural change of the endoplasmic reticulum during fertilization: evidence for loss of membrane continuity using the green fluorescent protein. Dev. Biol. *179*, 320–328.

Terasaki, M. (2000). Dynamics of the ER and Golgi apparatus during early sea urchin development. Mol. Biol. Cell *11*, 897–914.

Ward, G.E., and Kirschner, M.W. (1990). Identification of cell cycle-regulated phosphorylation sites on nuclear lamin C. Cell *61*, 561–577.

Weast, R.C. (ed.) (1972). Handbook of Chemistry and Physics. Cleveland, Ohio: The Chemical Rubber Co., F-47.

Yang, L., Guan, T., and Gerace, L. (1997). Integral membrane proteins of the nuclear envelope are dispersed throughout the endoplasmic reticulum during mitosis. J. Cell Biol. *137*, 1199–1210.

Zaal, K.J., Smith, C.L., Polishchuk, R.S., Altan, N., Cole, N.B., Ellenberg, J., Hirschberg, K., Presley, J.F., Roberts, T.H., Siggia, E., Phair, R.D., and Lippincott-Schwartz, J. (1999). Golgi membranes are absorbed into and reemerge from the ER during mitosis. Cell *99*, 589–601.